TORC1 Inhibits GSK3-Mediated Elo2 Phosphorylation to Regulate Very Long Chain Fatty Acid Synthesis and Autophagy

Cell Reports
Article

TORC1 Inhibits GSK3-Mediated Elo2 Phosphorylation to Regulate Very Long Chain Fatty Acid Synthesis and Autophagy

Christine Zimmermann,[1] Aline Santos,[2] Kenneth Gable,[3] Sharon Epstein,[2] Charulatha Gururaj,[4] Pierre Chymkowitch,[1] Dennis Pultz,[5] Steven V. Rødkær,[5] Lorena Clay,[6] Magnar Bjørås,[1] Yves Barral,[6] Amy Chang,[4] Nils J. Færgeman,[5] Teresa M. Dunn,[3] Howard Riezman,[2] and Jorrit M. Enserink[1,*]

[1]Department of Microbiology, Oslo University Hospital, and University of Oslo, 0027 Oslo, Norway
[2]Department of Biochemistry and NCCR Chemical Biology, University of Geneva, CH-1211 Geneva, Switzerland
[3]Department of Biochemistry and Molecular Biology, Uniformed Services University of the Health Sciences, Bethesda, MD 20814, USA
[4]Department of Molecular, Cellular and Developmental Biology, University of Michigan, Ann Arbor, MI 48109, USA
[5]Department of Biochemistry and Molecular Biology, University of Southern Denmark, DK-5230 Odense M, Denmark
[6]Institute of Biochemistry, Department of Biology, Eidgenössische Technische Hochschule (ETH), CH-8093 Zurich, Switzerland
*Correspondence: jorrit.enserink@rr-research.no
http://dx.doi.org/10.1016/j.celrep.2013.10.024

SUMMARY

Very long chain fatty acids (VLCFAs) are essential fatty acids with multiple functions, including ceramide synthesis. Although the components of the VLCFA biosynthetic machinery have been elucidated, how their activity is regulated to meet the cell's metabolic demand remains unknown. The goal of this study was to identify mechanisms that regulate the rate of VLCFA synthesis, and we discovered that the fatty acid elongase Elo2 is regulated by phosphorylation. Elo2 phosphorylation is induced upon inhibition of TORC1 and requires GSK3. Expression of nonphosphorylatable Elo2 profoundly alters the ceramide spectrum, reflecting aberrant VLCFA synthesis. Furthermore, VLCFA depletion results in constitutive activation of autophagy, which requires sphingoid base phosphorylation. This constitutive activation of autophagy diminishes cell survival, indicating that VLCFAs serve to dampen the amplitude of autophagy. Together, our data reveal a function for TORC1 and GSK3 in the regulation of VLCFA synthesis that has important implications for autophagy and cell homeostasis.

INTRODUCTION

Cells have developed mechanisms that sense environmental alterations and generate responses that maintain cellular homeostasis. A major challenge to homeostasis is nutrient availability. Cells detect changes in nutrient availability and activate signal transduction pathways that produce an integrated response that rewires cell metabolism and mobilizes new energy sources (De Virgilio and Loewith, 2006).

The kinase Target of Rapamycin (TOR) plays a central role in the cellular nutrient response. Two TOR homologs have been identified in *Saccharomyces cerevisiae*, Tor1 and Tor2 (Kunz et al., 1993), which associate with several proteins to form two distinct functional complexes: TOR complex 1 (TORC1) and TORC2. TORC2 is insensitive to rapamycin and contains Tor2, Avo1, Avo2, Avo3, Bit61, and Lst8. Relatively little is known about TORC2, except that it controls the actin cytoskeleton and sphingolipid biosynthesis (Aronova et al., 2008; Cybulski and Hall, 2009; Tabuchi et al., 2006). The rapamycin-sensitive TORC1, which consists of Kog1, Lst8, Tco89, and Tor1 or Tor2 (Loewith et al., 2002), strongly depends on nutrient availability, in particular nitrogen (Barbet et al., 1996). Under nutrient-rich conditions, TORC1 promotes growth-related processes like protein synthesis, ribosome biogenesis, and tRNA synthesis, while inhibiting catabolic processes like autophagy (De Virgilio and Loewith, 2006).

Macroautophagy (here referred to as autophagy) is a major cellular response triggered by multiple stimuli (He and Klionsky, 2009). It involves the delivery of cytoplasmic components to the yeast vacuole for degradation, thereby generating an internal pool of molecules that can be used for metabolism. TORC1 inhibits autophagy when nutrient levels are sufficient. However, under conditions of low nutrient availability, TORC1 activity is downregulated, leading to induction of autophagy (Noda and Ohsumi, 1998). Rapamycin treatment mimics nitrogen depletion and induces autophagy even in the presence of nutrients (Noda and Ohsumi, 1998).

Under nutrient-rich conditions, TORC1 inhibits autophagy by phosphorylating Atg13, thereby preventing its association with the kinase Atg1 (Kamada et al., 2000). Under conditions of low nutrient availability, downregulation of TORC1 leads to dephosphorylation of Atg13, causing it to bind and activate Atg1. Atg1

then induces formation of the autophagosome at the phagophore assembly site (He and Klionsky, 2009).

In mammalian cells, autophagy can also be activated by phosphorylated sphingosine, potentially through downregulation of TORC1, but the mechanism remains poorly defined (Lavieu et al., 2006; Young et al., 2013). Sphingoid bases, also known as long chain bases (LCBs), are best known as backbones of ceramides. Ceramides, which are structural constituents of eukaryotic membranes, also contain a VLCFA in addition to the LCB backbone. The LCBs in yeast are sphinganine (dihydrosphingosine [DHS]) and 4OH-sphinganine (phytosphingosine [PHS]). LCBs are synthesized by condensing palmitoyl-CoA with serine by serine palmitoyltransferase (SPT) to form 3-ketosphinganine, which is subsequently converted into DHS by Tsc10 and then hydroxylated by Sur2 to form PHS (Figure S1A). LCBs can be phosphorylated by Lcb4 and to a lesser extent by Lcb5 (Nagiec et al., 1998), and LCBs and phosphorylated LCBs (LCBPs) are signaling molecules (Dickson, 2008). PHS and DHS can be condensed with very long chain acyl-CoA by ceramide synthase to form dihydroceramide and phytoceramide, which are further processed to yield more complex sphingolipids.

Sphingolipid synthesis is carefully regulated by the cell, and a correct balance of LCBs, VLCFAs, and ceramide is crucial for cell viability (Kobayashi and Nagiec, 2003). The activity of SPT is one of the control points in sphingolipid synthesis, and several recent publications have identified Orm1 and Orm2 as targets of a feedback mechanism that regulates SPT (Breslow et al., 2010; Han et al., 2010). When LCB levels are sufficiently high, unphosphorylated Orm1/2 bind and inhibit SPT. However, when sphingolipid levels are low, the adaptor proteins Slm1 and Slm2 recruit the kinases Ypk1 and Ypk2 to a TORC2-containing plasma membrane compartment, where they are phosphorylated and activated by TORC2 and Pkh1/2 kinases (Berchtold et al., 2012; Niles et al., 2012). Ypk1/2 subsequently phosphorylates Orm1/2, relieving their inhibition of SPT, which synthesizes LCBs (Berchtold et al., 2012; Roelants et al., 2011).

The rate of LCB synthesis is strongly affected by the supply of VLCFAs; a low rate of VLCFA synthesis leads to accumulation of LCBs, which is detrimental to cell survival (Kobayashi and Nagiec, 2003). VLCFA synthesis takes place at the endoplasmic reticulum (ER) in a four-step biochemical cycle (Figure S1A; Nugteren, 1965): First, malonyl-CoA is condensed with an acyl-CoA precursor; the resulting 3-keto intermediate is then reduced; the 3-hydroxy species is dehydrated; and finally the enoyl product is reduced to yield a saturated fatty acid (FA) chain that is two carbons longer than its precursor. This cycle is repeated several times to yield C22, C24, and C26 FAs, which are the most prevalent yeast VLCFAs. The length of the carbon chain is determined by the FA elongase proteins (Elops) Elo2 and Elo3 (Denic and Weissman, 2007; Oh et al., 1997).

Surprisingly, while significant progress has been made in elucidating the mechanisms that regulate LCB synthesis, it remains unknown how the rate of VLCFA synthesis is controlled. In addition, although defects in VLCFA synthesis result in elevated LCB levels that lead to reduced cell survival (Kobayashi and Nagiec, 2003), the underlying cause of this survival defect remains unclear. In this study, we describe a molecular mechanism that regulates VLCFA synthesis to maintain cellular homeostasis.

RESULTS

Phosphorylation of Elo2 Is Important for its Activity

The molecular mechanisms that regulate fatty acid elongation remain unknown. To gain insight into regulation of the FA elongation cycle, we systematically searched for posttranslational modifications of proteins involved in this process using mass spectrometry (MS). Interestingly, we found that Elo2 was phosphorylated on three conserved residues in its C terminus, i.e., T334, S336, and S338 (Figures 1A, 1B, S1B, and S1C). Elo2 homologs in *S. pombe*, humans, and mice have also been found to be phosphorylated on corresponding residues in phosphoproteomic studies (Daub et al., 2008; Villén et al., 2007; Wilson-Grady et al., 2008), indicating that Elo2 phosphorylation is evolutionarily conserved.

To confirm our MS data, we analyzed Elo2 mobility on a Phostag gel (Kinoshita et al., 2006). A slower migrating Elo2 band was detected that disappeared after λ phosphatase treatment, demonstrating it corresponds to phosphorylated Elo2 (Figure 1C). Approximately 10% of Elo2 was phosphorylated in log phase cells under rich growth conditions. No slower migrating band could be detected in cells expressing the *elo2^{3A}* allele, which encodes a form of Elo2 in which T334, S336, and S338 are mutated to alanine, showing that Elo2 is phosphorylated on one or several of these residues (Figure 1D; expression levels of this mutant were reduced, see below).

To begin analyzing the relevance of Elo2 phosphorylation, we crossed an *elo2^{3A}* mutant with an *elo3Δ* deletion mutant. While either *ELO2* or *ELO3* can be deleted individually, the double mutant is not viable (Revardel et al., 1995). Interestingly, tetrad analysis showed that approximately 36% of *elo2^{3A} elo3Δ* double-mutant spores were not viable, whereas double mutants that did form a colony had a very slow growth phenotype (Figure 1E; data not shown). *elo2^{3A} elo3Δ* double mutants were also more sensitive to various types of stress, including heat stress (Figure S1D). These data indicate that Elo2 phosphorylation is important for its activity.

Phosphorylation of Elo2 Contributes to Balanced LCB and Ceramide Synthesis

To gain further insight in the physiological importance of Elo2 phosphorylation, we analyzed the sphingolipid spectrum by MS (Figure 2; Table S2). In wild-type (WT) cells, ceramides mostly contained VLCFA moieties with a chain length of 26 carbons (Figure 2A), and complex sphingolipids IPC, MIPC, and $M(IP)_2C$ mainly consisted of a total number of 44 carbons (Figures 2B–2D). In contrast, *elo2Δ* and *elo3Δ* single mutants showed strong reductions in VLCFA chain lengths (Figure 2A). Interestingly, VLCFA chain lengths in the *elo2^{3A}* mutant were also reduced, indicating that phosphorylation of Elo2 is important for VLCFA synthesis. VLCFA moieties in ceramides were shortest in the *elo2^{3A} elo3Δ* double mutant and mainly consisted of C14 FA chains (Figure 2A). Furthermore, VLCFA chains of complex sphingolipids in the *elo2^{3A} elo3Δ* double mutant were also shorter than in either of the *elo2^{3A}* and *elo3Δ* single mutants (Figures 2B–2D), which supports the idea that Elo2 and Elo3 have partially nonredundant functions in VLCFA synthesis. In addition, the total amounts of ceramides and complex

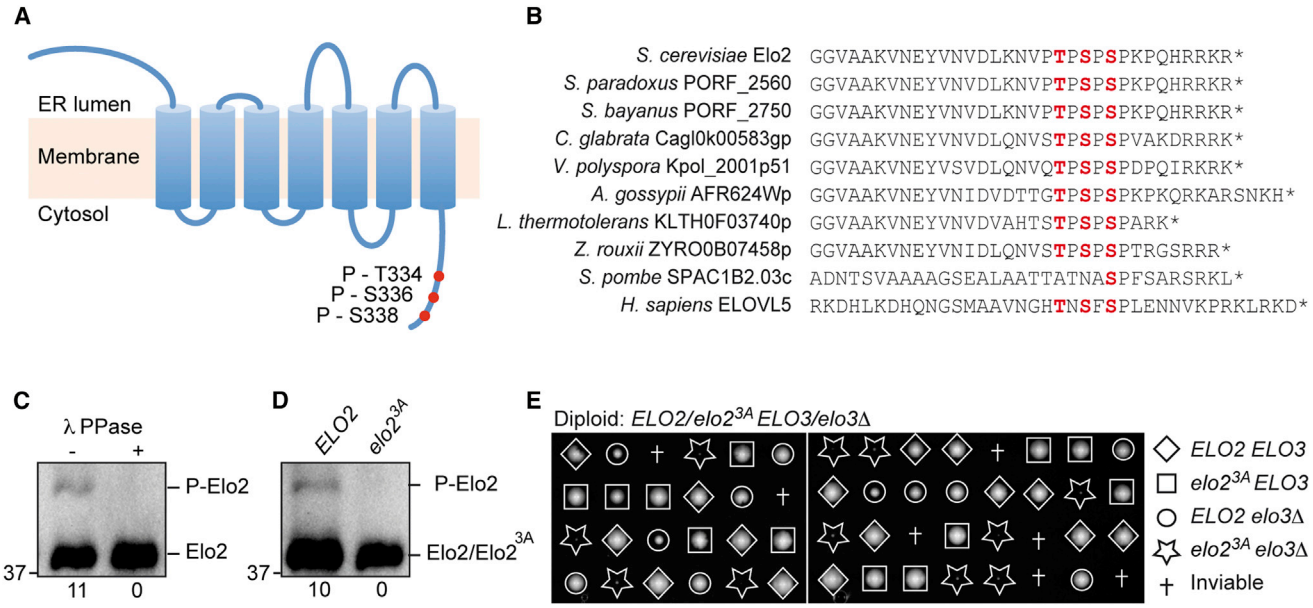

Figure 1. Phosphorylation of Elo2

(A) Graphical representation of the ER transmembrane protein Elo2.

(B) Elo2 phosphorylation sites are highly conserved.

(C) Elo2 is a phosphoprotein. Elo2-9Myc was immunoprecipitated, incubated with λ phosphatase, and analyzed by Phos-tag SDS-PAGE and anti-Myc western blotting. Numbers below the graph indicate the percentage of phosphorylated Elo2.

(D) Elo2^{3A} is not phosphorylated in vivo. Elo2 phosphorylation was analyzed as in (B).

(E) Tetrad dissection of spores derived from an *ELO2/elo2^{3A} ELO3/elo3Δ* diploid.

sphingolipids were generally reduced in the *elo2Δ*, *elo2^{3A}*, *elo3Δ* single mutants as well as in the *elo2^{3A} elo3Δ* double mutant (Table S2), which is in accordance with a previous study that analyzed sphingolipid levels in *elo2Δ* and *elo3Δ* mutants (Ejsing et al., 2009). Because the total amounts of lipids were highly reduced (particularly the C44:0 species in *elo2Δ* and *elo2^{3A}* mutants; Figures 2C and 2D), the *relative* contribution of otherwise minor abundant lipids such as C46:0 appeared to be increased, even though their absolute levels were strongly reduced in comparison with WT cells (Table S2). These data indicate that phosphorylation of Elo2 also affects the flux by which different lipids are synthesized.

Finally, we analyzed cellular phospholipid content and found that while phospholipid composition was unaffected (Figure S2A), mutations in *ELO2* and *ELO3* resulted in altered acyl chain composition (Table S2). Together, our data demonstrate that Elo2 phosphorylation contributes to maintaining the cellular sphingolipid balance and the *elo2^{3A}* phenotype is intermediate between the WT and null alleles.

Reducing the Synthesis of LCBs and LCBPs Promotes Survival of *elo2^{3A} elo3Δ* Mutants

It has previously been shown that reduced VLCA synthesis results in imbalances in LCB levels, which are toxic to cells (Kobayashi and Nagiec, 2003). To gain insight into the possible effect of Elo2 phosphorylation on LCB levels, we directly analyzed free LCBs. Interestingly, *elo2^{3A}* and *elo3Δ* single mutants, but particularly *elo2^{3A} elo3Δ* double mutants, all had increased levels of free LCBs (Figure 3A; Table S3). These mutants also showed strongly increased levels of LCBPs (Figure 3B), indicating that Elo2 phosphorylation prevents accumulation of LCBs and LCBPs.

Based on these findings, we speculated that the slow-growth phenotype of the *elo2^{3A} elo3Δ* double mutant might be caused by LCB accumulation. Indeed, low doses of myriocin (an antibiotic that inhibits SPT, the first step in LCB production) substantially improved growth of the *elo2^{3A} elo3Δ* double mutant (Figure 3C), which was at least in part due to increased cell survival (Figure S2B). Consistently, expression of *lcb1-C180W*, a dominant-negative allele of *LCB1* that moderately inhibits SPT activity (Gable et al., 2002), also improved growth and survival of this mutant (Figures S2C and 2D). These data support the hypothesis that defects in VLCFA synthesis result in unbalanced LCB synthesis, impairing cell survival.

Because reducing the rate of LCB synthesis improved growth and survival of *elo2^{3A} elo3Δ* mutants, we predicted that increasing the rate of LCB synthesis should have the opposite effect. Deletion of *ORM2* has previously been shown to increase LCB synthesis by SPT (Breslow et al., 2010; Han et al., 2010). Accordingly, although *elo2^{3A} orm2Δ* and *elo3Δ orm2Δ* double mutants were viable (Figure 3D), an *elo2^{3A} elo3Δ orm2Δ* triple mutant was only viable when cells contained a plasmid harboring *ORM2* (Figure 3E). Thus, increasing the activity of SPT by deletion of *ORM2* promotes cell death of *elo2^{3A} elo3Δ* mutants.

The phosphorylation state of the Orm proteins is under feedback regulation by downstream intermediates in the sphingolipid synthesis pathway (Breslow et al., 2010; Liu et al., 2012). When LCB levels are low, for example after myriocin treatment, Orm1

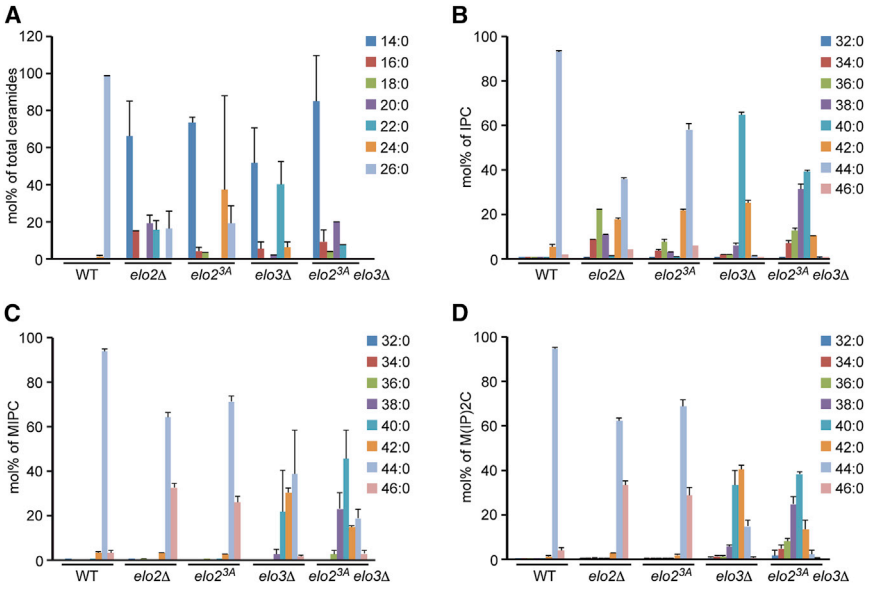

Figure 2. Phosphorylation of Elo2 Is Important for Elo2 Activity

(A) Accumulation of ceramide species with shortened fatty acyl moieties in *elo2* and *elo3Δ* mutants. Data are presented as mol% of total ceramides and organized by fatty-acyl chain lengths.

(B–D) Preventing Elo2 phosphorylation leads to accumulation of ceramides with short-chain fatty acyl chains. Complex sphingolipids are represented as the sum of the number of carbons of the sphingoid base and the fatty acid, and data are presented as mol% of each lipid class, i.e., IPC (B), MIPC (C), and M(IP)2C (D). Average values of three independent biological replicates are shown; error bars represent SD (note that due to experimental variation between each experiment, the total value of lipids may appear to exceed 100%; for data of individual experiments, see Table S2).

becomes hyperphosphorylated, thereby relieving inhibition of SPT (Breslow et al., 2010; Liu et al., 2012). We have previously shown that multiple forms of Orm1 exist in the cell (unphosphorylated, hypophosphorylated, and hyperphosphorylated Orm1) and that myriocin primarily induces hyperphosphorylation (Liu et al., 2012). Consistent with our previous findings, approximately 8% of the Orm1 population was hyperphosphorylated under basal conditions in WT cells, which increased to 78% after treatment with myriocin (Figure 3F). In contrast, under basal conditions, no hyperphosphorylated Orm1 could be detected in *elo2^{3A}* mutants. Furthermore, myriocin treatment resulted in much lower levels of hyperphosphorylated Orm1 (42%) in *elo2^{3A}* mutants than in WT cells. Myriocin-induced Orm1 hyperphosphorylation did not occur at all in either *elo3Δ* single mutants or in *elo2^{3A} elo3Δ* double mutants (Figure 3F). These data indicate that preventing Elo2 phosphorylation reduces the activity of signaling pathways that target Orm1p, most likely as a result of accumulation of intermediates in the sphingolipid synthesis pathway.

LCBs are mainly phosphorylated by Lcb4 (Nagiec et al., 1998). Because accumulation of LCBPs is particularly toxic to cells (Kim et al., 2000), we tested the effect of preventing LCB phosphorylation on growth of *elo2^{3A} elo3Δ* double mutants. Interestingly, deletion of *LCB4* improved growth of *elo2^{3A} elo3Δ* mutants (Figure 3G). Conversely, deletion of *DPL1*, which encodes the major enzyme that degrades LCBPs (Saba et al., 1997), caused reduced growth of *elo2^{3A}* mutant cells (Figure S2E) and synthetic lethality in an *elo3Δ* background (J.M.E., unpublished data; Aguilar et al., 2010).

Taken together, these data indicate that Elo2 is regulated by phosphorylation and that accumulation of LCBs and LCBPs impairs survival of *elo2^{3A} elo3Δ* double mutants.

Reduced VLCFA Synthesis Activates Autophagy in an LCBP-Dependent Manner

What causes the strongly reduced cell growth and survival of *elo2^{3A} elo3Δ* mutants? Previously, we found that inhibition of FA synthase induces a starvation response (Pultz et al., 2012). A major aspect of this response is autophagy (Kamada et al., 2000). Thus, we hypothesized that autophagy might be activated in *elo2^{3A} elo3Δ* mutants. We studied autophagy by monitoring the behavior of the GFP-Atg8 reporter under the control of the *ATG8* promoter (He and Klionsky, 2009).

First, we examined the localization of GFP-Atg8 to the vacuole, a commonly used autophagy assay (Cheong and Klionsky, 2008). When grown in media containing nitrogen, the GFP-Atg8 signal was primarily diffuse and cytoplasmic both in WT cells and in *elo2^{3A}* single mutants, while vacuolar staining could be detected in approximately 8% of the cells, which increased to approximately 78% upon nitrogen starvation (Figure 4A). Interestingly, the number of autophagic cells was significantly higher in the *elo3Δ* mutant (Figure 4A); moreover, *elo2^{3A} elo3Δ* double mutants showed a synergistic increase in the percentage of autophagic cells (62%), showing that combined activity of Elo2 and Elo3 is required to suppress autophagy under nitrogen-rich conditions. During nitrogen starvation, the number of autophagic *elo2^{3A} elo3Δ* double mutant cells was also significantly higher than WT cells. As expected, autophagy in these mutants was entirely dependent on *ATG1* and *ATG7* (Figure 4B; C.Z., unpublished data).

We also monitored autophagic flux, which is the vacuolar transfer and degradation of autophagosomes over time, using a GFP-Atg8 processing assay (Cheong and Klionsky, 2008). This assay exploits the fact that part of the Atg8 pool is present in the interior of autophagosomes, and this pool is transported into the vacuole lumen. Vacuolar hydrolases cleave the GFP-Atg8 fusion protein to release free GFP, which has a relatively long half-life in the vacuole interior and which can be detected by western blotting. Interestingly, even under nutrient-rich conditions, autophagic flux was approximately four times higher in the *elo2^{3A} elo3Δ* double mutant than in WT cells (compare lanes 1 and 10 in Figure S3A; quantified in Figure S3B), which is consistent with our GFP-Atg8 localization data. We conclude that the autophagic flux in *elo2^{3A} elo3Δ* double-mutant cells is increased even under nutrient-rich conditions.

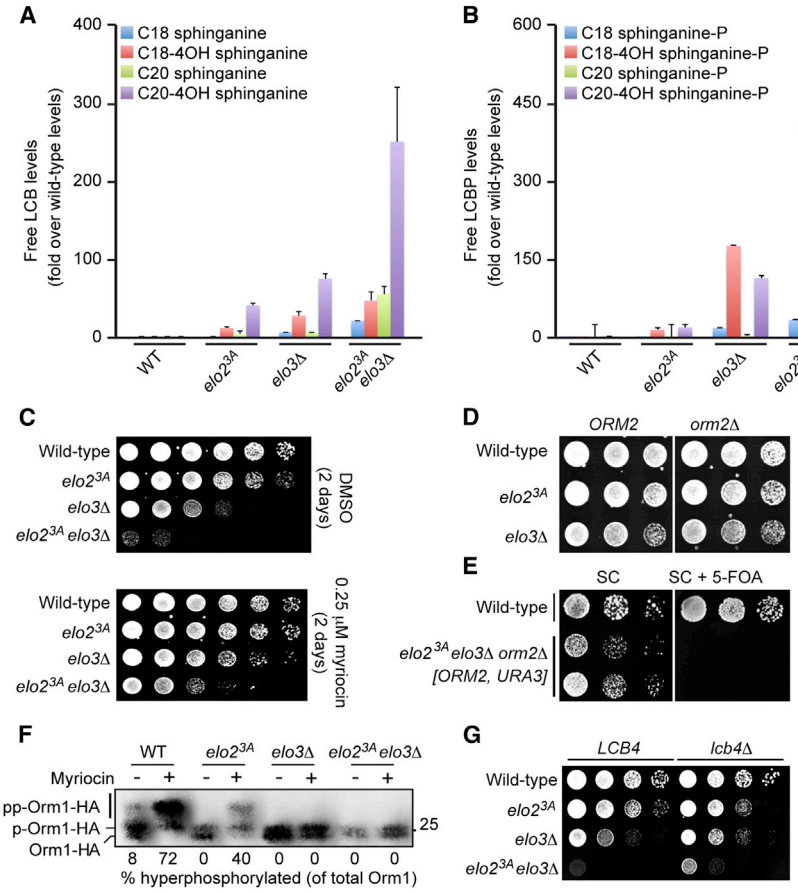

Figure 3. Accumulation of LCBs in *elo2* and *elo3* Mutants Impairs Cell Viability

(A and B) Accumulation of LCBs and LCBPs in *elo2* and *elo3Δ* mutants. LCBs (A) and LCBPs (B) were detected by liquid chromatography MS. Data are normalized to the levels observed in WT cells.

(C) Slow growth of $elo2^{3A}$ *elo3Δ* mutants can be rescued by low doses of myriocin.

(D and E) Synthetic lethal phenotype of the $elo2^{3A}$ *elo3Δ orm2Δ* mutant. Spot assays of WT, *orm2Δ* single mutants, and $elo2^{3A}$ *orm2Δ* and *elo3Δ orm2Δ* double mutants (D). Plasmid shuffle with $elo2^{3A}$ *elo3Δ orm2Δ* triple-mutant cells harboring an *URA3*-based plasmid containing *ORM2* shows inviability on 5-FOA (E). WT control: strain RDKY3023, which is ura^{-}.

(F) Diminished myriocin-induced Orm1 phosphorylation in $elo2^{3A}$ mutant cells. Strains were treated with myriocin and Orm1 phosphorylation was analyzed by western blotting. pp-Orm1, hyperphosphorylated Orm1; p-Orm1, hypophosphorylated Orm1; and Orm1, unphosphorylated Orm1.

(G) Deleting *LCB4* improves the growth of $elo2^{3A}$ *elo3Δ* double mutants.

Autophagy was also monitored by following the vacuolar localization of aminopeptidase I (Ape1). Ape1 is selectively transported into the vacuole via the cytoplasm-to-vacuole targeting pathway under vegetative conditions and via autophagy under starvation conditions (Baba et al., 1997). GFP-Ape1 was present in cytoplasmic foci in approximately 70% of the WT cells, while 30% of the cells had vacuolar GFP-Ape1 (Figure S3C). The pattern of GFP-Ape1 localization in $elo2^{3A}$ single-mutant cells was similar to WT cells. In contrast, GFP-Ape1 localized to the vacuole in approximately 70% of the *elo3Δ* single mutants and in 97% of the $elo2^{3A}$ *elo3Δ* double-mutant cells (Figure S3C). These data show that reduced VLCFA synthesis triggers autophagy.

To determine whether constitutive activation of autophagy underlies the slow-growth phenotype of $elo2^{3A}$ *elo3Δ* double mutants, we deleted *ATG1* in this genetic background. Strikingly, deletion of *ATG1* considerably improved growth of both the *elo3Δ* single mutant and the $elo2^{3A}$ *elo3Δ* double mutant (Figure 4C). Similar results were obtained when we deleted *ATG7* (Figure 4D). Thus, the strong growth defect of $elo2^{3A}$ *elo3Δ* mutant is at least in part caused by constitutive autophagy.

If excessive autophagy indeed causes reduced survival of $elo2^{3A}$ *elo3Δ* mutants, then deletion of *SCH9*, which encodes a kinase that inhibits autophagy (Yorimitsu et al., 2007), should result in an aggravated growth phenotype. Indeed, deletion of *SCH9* reduced growth of both $elo2^{3A}$ and *elo3Δ* singe mutants (Figure S3D), and we were unable to isolate any *sch9Δ* $elo2^{3A}$ *elo3Δ* triple mutants by tetrad dissection (not shown). A limitation of tetrad dissection is that only a relatively small number of tetrads can be analyzed simultaneously, in particular because 36% of $elo2^{3A}$ *elo3Δ* double-mutant spores are not viable (Figure 1E). Therefore, we resorted to bulk segregation analysis (Michelmore et al., 1991). We randomly isolated spores from an *ELO2*/$elo2^{3A}$ *ELO3*/*elo3Δ SCH9*/*sch9Δ* diploid strain, which gave rise to 1,164 unique colonies on double selection plates that contained a combination of nourseothricin and hygromycin (thus selecting for $elo2^{3A}$ *elo3Δ* double mutants only). Because the *ELO2*, *ELO3*, and *SCH9* loci are not syntenic, the WT *SCH9* allele and the *sch9Δ* mutation should segregate in a Mendelian ratio of 1:1, and therefore half of the 1,164 isolates should contain the *sch9Δ* deletion. However, not one of the 1,164 offspring was *sch9Δ*. This strongly implies that *SCH9* is essential for survival of $elo2^{3A}$ *elo3Δ* cells. One explanation for these results is that *SCH9* is essential for suppressing excessive autophagy in this mutant.

What is the signal that triggers autophagy? Because we found that increased LCB and LCBP levels contributed to the reduced survival of the $elo2^{3A}$ *elo3Δ* mutant, we hypothesized that LCBs or LCBPs might activate autophagy. Treatment of WT cells with increasing doses of exogenous PHS resulted in a significant increase in the number of cells undergoing autophagy (Figure S3E), indicating that PHS is sufficient to induce autophagy. If accumulation of LCBs is responsible for autophagy in $elo2^{3A}$ *elo3Δ* mutants, then treatment with myriocin should inhibit autophagy. Indeed, autophagy was modestly but significantly reduced when

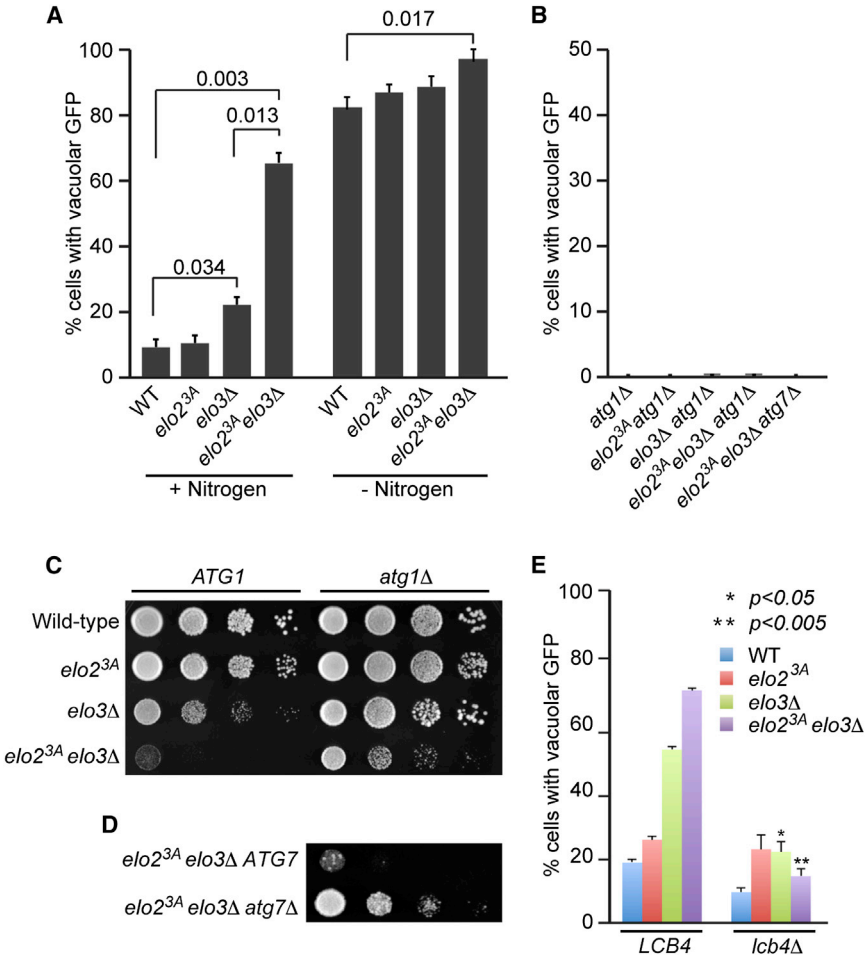

Figure 4. Constitutive Activation of Autophagy Reduces Viability of *elo2^{3A} elo3Δ* Double Mutants

(A) Vacuolar localization of GFP-Atg8. Cells were grown to log phase in SC medium with nitrogen and either maintained in SC with nitrogen ("+ Nitrogen") or transferred to SC without nitrogen for 3 hr ("− Nitrogen"), after which GFP-Atg8 localization was quantified by fluorescence microscopy.

(B) *ATG1* and *ATG7* are required for autophagy in *elo* mutants. Cells were grown to log phase in synthetic medium with nitrogen and analyzed as in (A).

(C and D) Preventing autophagy by deleting *ATG1* (C) or *ATG7* (D) promotes survival of *elo2^{3A} elo3Δ* mutants.

(E) Deletion of *LCB4* suppresses autophagy in *elo2^{3A} elo3Δ* mutants. Autophagy was measured as in (A).

Error bars indicate SD. Numbers indicate p values (Student's t test).

cells were grown in the presence of 1 μM myriocin (Figure S3F). This dose of myriocin is not sufficient to fully inhibit SPT, but higher doses could not be tested due to severe impairment of cell survival, which confounded the results (Figure S2B; C.Z., unpublished data). We also analyzed autophagy in strains transformed with an empty vector or with plasmids containing either WT *LCB1* or dominant-negative *lcb1-C180W* (both under control of the *LCB1* promoter). Interestingly, providing additional copies of *LCB1* significantly increased autophagy in the *elo2^{3A} elo3Δ* mutant, while expression of the *lcb1-C180W* allele resulted in decreased autophagy (Figure S3G).

Finally, we studied the effect of Lcb4 on autophagy, because deletion of *LCB4* improved the growth of the *elo2^{3A} elo3Δ* mutant (Figure 3G). Strikingly, deletion of *LCB4*, but not *LCB5*, strongly reduced autophagy in *elo3Δ* and *elo2^{3A} elo3Δ* mutants (Figure 4E; data not shown). Conversely, deletion of *DPL1* significantly increased autophagy in *elo2^{3A}* single-mutant cells (Figure S3H). These data strongly suggest that LCBs and LCBPs promote autophagy in *elo* mutants.

Together, these data show that (1) autophagy is constitutively active in mutants with defects in VLCFA synthesis, (2) phosphorylation of Elo2 helps prevent excessive activation of the autophagy pathway, (3) constitutive activation of autophagy is detrimental to survival of these mutants, and (4) cells may sense LCBPs as a proxy for VLCFA levels to activate autophagy.

Elo2 Phosphorylation Requires GSK3 and Is Inhibited by TORC1

Serendipitously, during sample preparation, we observed that Elo2 phosphorylation appeared to be increased when Elo2 was isolated from nutrient-depleted cells compared with cells grown in rich medium. Intrigued by this observation, we tested whether Elo2 phosphorylation responds to nutrient availability. Indeed, nitrogen depletion substantially increased Elo2 phosphorylation compared with cells grown in YPD (62% versus 12%; Figure 5A; see Figure S4A for loading controls). Phosphorylation of Elo2 was also increased after treatment with the TORC1 inhibitor rapamycin (78%). In contrast, neither FK506, which inhibits the phosphatase calcineurin, nor PHS had a strong effect on Elo2 phosphorylation. These data suggest that TORC1 inhibits Elo2 phosphorylation under nutrient-rich conditions.

The phosphorylated residues in Elo2 are all followed by prolines, indicating that a proline-directed kinase phosphorylates Elo2. We therefore screened all proline-directed kinases (MAPKs, CDKs, Yak1, and Kns1) for an involvement in Elo2 phosphorylation. However, Elo2 phosphorylation was unaffected in mutants lacking any of these kinases (Figures S4B–S4D).

iGPS software (Song et al., 2012) predicted with high confidence that all three Elo2 phosphorylation sites resemble GSK3 consensus sites. Indeed, Elo2 phosphorylation was undetectable in a *ygk3Δ mck1Δ rim11Δ mrk1Δ* quadruple mutant (from hereon referred to as *gsk3Δ*), which lacks all four GSK3 kinases found in yeast (Figures 5B and 5C; see Figure S4E for loading controls), demonstrating that GSK3 regulates Elo2 phosphorylation in vivo. Consistent with this, overexpression of *MCK1* and

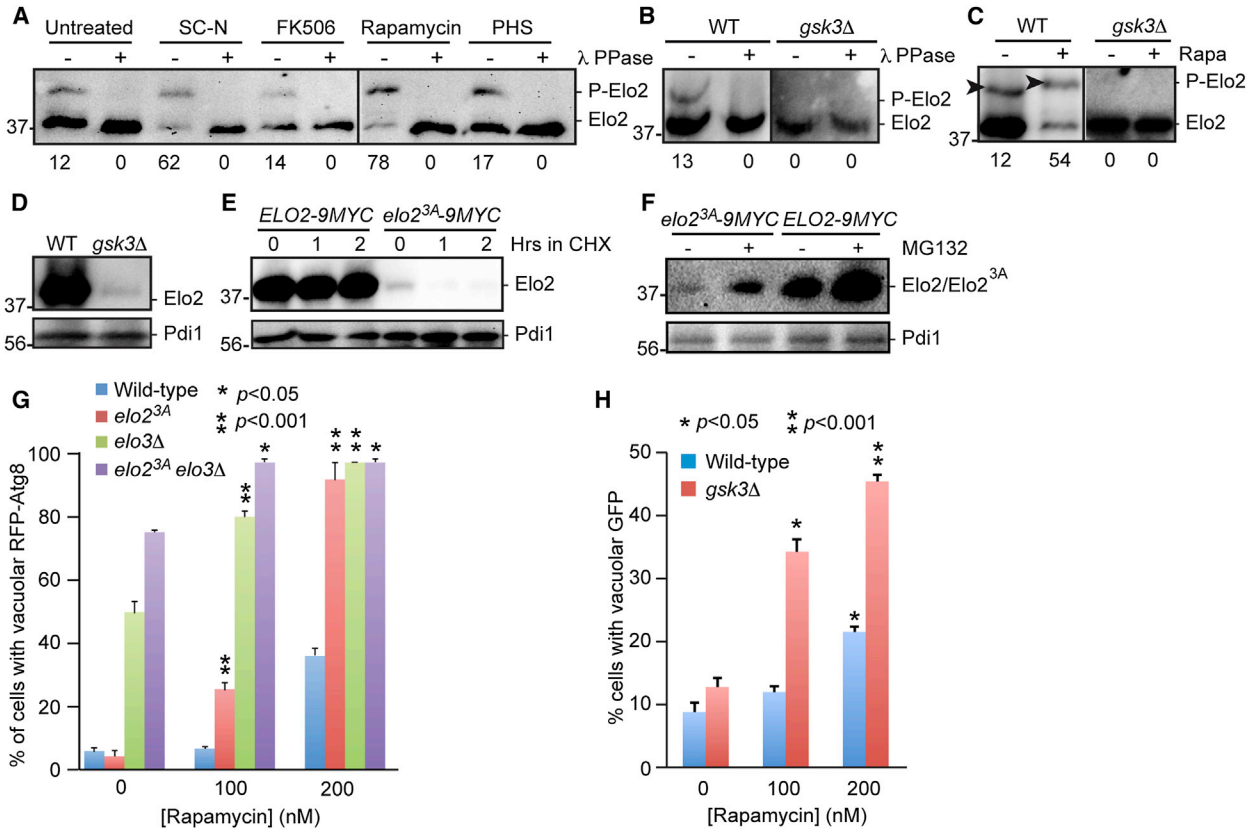

Figure 5. Elo2 Phosphorylation Is Positively Regulated by GSK3 and Negatively by TORC1

(A) Elo2 phosphorylation increases after nitrogen starvation and rapamycin treatment. Cells expressing Elo2-9Myc were grown to log phase in YPD and either transferred to SC-N for 3 hr or treated with 1 μM FK506, 1 μM rapamycin, or 25 μg/ml PHS for 1 hr. Elo2 phosphorylation was analyzed as in Figure 1C. Numbers below the graph indicate the percentage of phosphorylated Elo2. All samples were obtained from the same experiment but analyzed on two separate gels (indicated by dividing line).

(B) Elo2 phosphorylation depends on GSK3. Elo2 phosphorylation was analyzed in either WT cells or a mutant lacking all four GSK3 kinases. Numbers below the graph indicate the percentage of phosphorylated Elo2. The western blot showing Elo2 in the *gsk3Δ* strain had to be exposed longer due to reduced Elo2 levels.

(C) Rapamycin-induced Elo2 phosphorylation requires GSK3. WT cells and a mutant lacking all four GSK3 kinases were treated with 1 μM rapamycin for 1 hr and Elo2 phosphorylation was analyzed as described in Figure 1C. Numbers below the graph indicate the percentage of phosphorylated Elo2. The western blot showing Elo2 in the mutant strain was exposed longer due to reduced Elo2 levels in this mutant. Arrowheads indicate phosphorylated Elo2 (Elo2 immunoprecipitation samples often contain lipids that slightly distort Phos-tag gels).

(D) Reduced Elo2 expression levels in *gsk3Δ* mutants. Strains expressing Elo2-9Myc were grown to log phase and Elo2 levels were analyzed using conventional SDS-PAGE.

(E) Unphosphorylatable Elo2 is an unstable protein. Log phase *ELO2-9MYC* and *elo2^{3A}-9MYC* cultures were treated with cycloheximide (CHX) for the indicated times, and Elo2 stability was analyzed as in (D).

(F) Elo2^{3A} protein levels are partially restored by inhibiting the proteasome. Log phase cells were treated MG132 and Elo2 phosphorylation was analyzed as in (D).

(G) *elo2^{3A}* and *elo3Δ* mutants are sensitized to rapamycin-induced autophagy. Log phase cells were treated with 0, 100, or 200 nM rapamycin for 3 hr. The fraction of cells with vacuolar GFP-Atg8 was analyzed by fluorescence microscopy.

(H) *gsk3Δ* mutants are sensitized to autophagy. Autophagy was induced and analyzed as described in (G).

MRK1 induced hyperphosphorylation of Elo2 (data not shown). We screened single-deletion mutants lacking each of the four GSK3 isoforms and found that *MCK1* is responsible for most of the Elo2 phosphorylation (Figure S4F). A low level of Elo2 phosphorylation still occurred in an *mck1Δ* mutant, indicating that other GSK3 isoforms make minor contributions to Elo2 phosphorylation (Figure S4G). Some Elo2 phosphorylation could also be detected in a *mck1 ygk3 mrk1* triple mutant, whereas additional deletion of *RIM11* in this background resulted in loss of Elo2 phosphorylation and strongly reduced Elo2 levels (Figure S4H and see below).

Finally, since at least some of the effects of TORC1 are mediated by the PP2A-like phosphatase Sit4 (Broach, 2012), we determined whether Sit4 is involved in regulation of Elo2 phosphorylation. Interestingly, whereas 11% of Elo2 was phosphorylated under basal conditions in WT cells, deletion of *SIT4* reduced Elo2 phosphorylation to just 1% (Figure S4I). Furthermore, rapamycin-induced Elo2 phosphorylation was substantially lower in *sit4Δ* mutants than in WT cells (49% versus 92%). These data indicate that Sit4 promotes Elo2 phosphorylation. In contrast, simultaneous deletion of *PPH21* and *PPH22*, which encode PP2A phosphatases that have TORC1-dependent

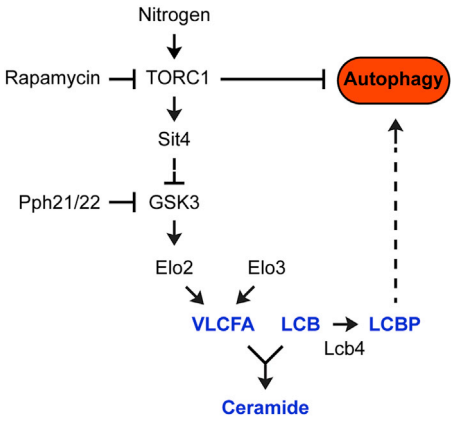

Figure 6. Model of the Findings in This Study
Blue indicates metabolic intermediates. See text for details.

and independent functions (Broach, 2012), resulted in increased Elo2 phosphorylation under basal conditions (Figure S4I), suggesting that these phosphatases may dephosphorylate Elo2.

Collectively, although the exact molecular mechanism remains to be determined, these data indicate that Sit4 and GSK3 promote Elo2 phosphorylation, whereas Pph21/22 may directly dephosphorylate Elo2.

Phosphorylation of Elo2 May Affect Protein Stability

How does phosphorylation affect Elo2 function? The ER localization of unphosphorylatable Elo2^{3A} was unaltered, indicating that phosphorylation does not affect Elo2 localization (Figure S4J). However, we noticed that Elo2 protein levels were strongly reduced in the *gsk3Δ* mutant compared to WT cells (Figure 5D, upper panel; Figure S4H). This was specific for Elo2, because the levels of Pdi1p, another ER-localized protein, were not affected (Figure 5D, lower panel). The effect of *GSK3* on Elo2 stability is likely to be direct, because the levels of nonphosphorylatable Elo2^{3A} protein were also strongly reduced (Figure 5E). Treatment with cycloheximide resulted in further depletion of Elo2^{3A} (Figure 5E), whereas treatment with the proteasome inhibitor MG132 resulted in partial recovery of Elo2^{3A} levels (Figure 5F). In contrast, Elo2 was not degraded by the autophagy pathway (Figure S4K). These data show that preventing Elo2 phosphorylation affects its proteasomal turnover.

Elops Dampen the Amplitude of Autophagy

To determine how Elo2 phosphorylation affects autophagy, we treated cells with low doses of rapamycin to slightly inhibit TORC1. First, we treated WT cells with increasing concentrations of rapamycin to determine at which dose autophagy is induced. Increased autophagy was only observed in WT cells after treatment with at least 200 ng/ml rapamycin (Figure S4L). However, autophagy was already significantly elevated at 100 ng/ml rapamycin in *elo2^{3A}* and *elo3Δ* single mutants and in *elo2^{3A} elo3Δ* double mutants (Figure 5G). Consistent with this, *gsk3Δ* mutants were also sensitized to low doses of rapamycin (Figure 5H). Thus, *GSK3*-dependent phosphorylation of Elo2 dampens autophagy under conditions of partial TORC1 inhibition, indicating that VLCFA depletion sensitizes cells to autophagy.

DISCUSSION

VLCFA synthesis must be carefully regulated, because imbalances in VLCFAs have profound effects on LCB levels and cell viability (Kobayashi and Nagiec, 2003). However, the mechanism whereby cells control the rate of VLCFA synthesis has remained obscure until this study. Here, we report that VLCFA synthesis is at least in part dependent on phosphorylation of Elo2. Elo2 phosphorylation was negatively regulated by TORC1 and positively regulated by GSK3, and Mck1 was the main GSK3 isoform responsible for Elo2 phosphorylation (see Figure 6 for an overview of our findings).

Compared with mammals, very little is known about regulation of GSK3 kinases in yeast. Mammalian GSK3 is a substrate for several kinases including ribosomal S6 kinase, a downstream target of mTORC1 that phosphorylates GSK3 in its N terminus to inhibit its kinase activity (Zhang et al., 2006). Inhibition of mammalian GSK3 by the mTOR pathway is consistent with our finding that GSK3 is a downstream component of the rapamycin-sensitive TORC1 signaling pathway in yeast. Our results are also consistent with a recent yeast study that found that TORC1 inhibits Mck1 to regulate tRNA synthesis, although it remained unknown exactly how TORC1 regulates Mck1 (Lee et al., 2012).

Completely preventing Elo2 phosphorylation, either by deleting all GSK3 isoforms or by alanine substitution of the phosphorylation sites, resulted in strongly decreased Elo2 levels. This could be partially rescued with the proteasome inhibitor MG132, indicating that constitutive dephosphorylation of Elo2 leads to its proteasomal degradation. We do not exclude the possibility that there may be additional mechanisms by which phosphorylation regulates Elo2 activity. For instance, it could affect the composition of the protein complex involved in the fatty acid elongation cycle. Alternatively, it could regulate Elo2 catalytic activity, for example by regulating access of substrate to the catalytic site. The exact molecular mechanism by which Elo2 elongates fatty acids is currently unknown and probably will remain unknown until the crystal structure of an Elop bound to its substrate is solved. This structure may also reveal how phosphorylation of the C terminus affects Elo2 enzymatic activity.

We found that inhibiting VLCFA synthesis results in a dramatic loss of viability. It has been reported previously that inhibiting VLCFA synthesis results in reduced cell viability due to accumulation of LCBs (Kobayashi and Nagiec, 2003), although the underlying cause was never determined. In this study, we discovered that this reduced survival was at least partially caused by LCBP-mediated, constitutive activation of autophagy. Autophagy is a catabolic process aimed at degradation of cellular components, and while autophagy is well known to promote cell survival during starvation, it is likely that uncontrolled and excessive autophagy will ultimately deplete factors essential for cell survival.

What could be the physiological function of activation of autophagy by LCBPs in normal cells? Because LCBs and LCBPs

accumulate when VLCFA levels are low, and because LCBPs mediate activation of autophagy, we believe that cells may monitor LCBPs to sense the pool of free FAs. In this model, depletion of VLCFAs leads to an increase in LCBPs, which then trigger autophagy, and we speculate that autophagy serves to replenish cellular FA levels. Interestingly, a recent study showed that inhibition of TORC1 activates the kinase Npr1, which in turn phosphorylates and inhibits Orm1/2 to induce LCB synthesis (Liu et al., 2012; Shimobayashi et al., 2013). Thus, inhibition of TORC1 may promote ceramide synthesis by coordinately increasing the production of both VLCFA and LCBs. This increased ceramide synthesis, which takes place at the ER, might be important for supplying membrane material during autophagy. The source of membrane material for autophagy remains subject to debate, although the consensus is emerging that the ER is a major contributor (Orsi et al., 2010); therefore, one reason for increased ceramide synthesis could be to supply the ER with membrane material to sustain the autophagic process.

Although LCBPs are required for induction of autophagy in *elo2*^{3A} *elo3Δ* mutants, we currently do not know the molecular mechanism by which LCBPs activate autophagy. It is possible that intracellular receptors exist that induce autophagy upon binding to LCBPs. However, the yeast proteins that bind LCBs and LCBPs remain unknown. A recent study identified several proteins that may bind these lipids in vitro, including Slm1 and Atg18 (Gallego et al., 2010), but it is unclear whether these proteins actually bind LCBs and LCBPs in vivo. Alternatively, LCBPs may activate autophagy through a more indirect mechanism, for example by modulating cellular amino acid levels. We have indications that *elo2Δ* and *elo3Δ* mutants indeed have reduced amino acid pools (N.J.F., unpublished data). Clearly, additional studies are required to determine how LCBPs activate autophagy.

In conclusion, we discovered a molecular mechanism for regulation of VLCFA synthesis that has important implications for autophagy and cell homeostasis. Because Elo2 phosphorylation sites are highly conserved and phosphorylation of the Elo2-related FA elongase ELOVL5 has been observed in phosphoproteomic studies of mouse liver and human cell lines (Daub et al., 2008; Villén et al., 2007), the regulatory mechanism of VLCFA synthesis may be conserved among eukaryotes.

EXPERIMENTAL PROCEDURES

Strains, Plasmids, and Growth Conditions

S. cerevisiae strains were grown in standard YPD medium unless indicated otherwise. Strains were directly derived from the S288c strains RDKY3032 and RDKY3615 (Enserink et al., 2009; Flores-Rozas and Kolodner, 1998), except the *gsk3Δ* mutant that was derived from W303, and all strains were constructed using either standard gene replacement methods or by intercrossing (see Table S1 for strains and plasmids).

Analysis of Elo2 Phosphorylation

Elo2 was purified as previously described (Denic and Weissman, 2007). Briefly, 50 ml log phase culture was washed with ice-cold water and lysed by bead beating for 10 min in 2 ml buffer A (50 mM HEPES [pH 6.8], 150 mM KAc, 2 mM $MgAc_2$, 1 mM $CaCl_2$, 200 mM Sorbitol, 1 mM Na_3VO_4, 10 mM NaF, and fungal protease inhibitor cocktail, according to the manufacturer's instructions; Calbiochem). Lysates were centrifuged for 10 min (5,000 × *g*, 4°C), insoluble debris was discarded, and soluble fraction was centrifuged (40 min, 40,000 × *g*, 4°C) to isolate microsomes. Microsomes were solubilized in 600 μl ice-cold buffer B (buffer A supplemented with 0.5% sodium deoxycholate and 0.5% Tergitol/NP-40). Elo2-9Myc was immunoprecipitated with anti-Myc beads for 2–3 hr at 4°C, washed four times with 1 ml buffer B, and eluted in Laemmli sample buffer. Elo2 phosphorylation was assessed by Phos-tag SDS-PAGE (Kinoshita et al., 2006) followed by western blotting with Myc antibodies.

λ Phosphatase Treatments

Elo2-9Myc was purified as described above, washed three times with 1 ml λ buffer (150 mM NaCl, 50 mM Tris-HCl [pH 7.5], 1 mM EDTA, 50 mM DTT, 0.01% Tergitol/NP40, and protease inhibitor cocktail) and resuspended in 100 μl λ buffer. The samples were split in two, 1.5 μl of λ phosphatase (400,000 U/ml) was added to one of the samples, and both samples were incubated at 30°C for 1 hr (vortexed 5 s every 3 min). Elo2 phosphorylation was analyzed as described above.

Elo2 Stability

Cycloheximide treatment was performed as previously described (Zimmermann et al., 2011). Log phase *ELO2-9Myc* and *elo2*^{3A}*-9Myc* strains were treated with 400 μg/ml cycloheximide for 0, 30, 60, and 120 min.

MG132 treatment was carried out as previously described (Liu et al., 2007). To permeabilize cells, 0.003% SDS was added for 3 hr to log phase cultures, after which cells were incubated for 2 hr with 100 μM MG132. Elo2 was purified as described above and analyzed by conventional SDS-PAGE.

Mass Spectrometry

Mapping of phosphorylation sites by MS was carried out as previously described (Pultz et al., 2012).

Analysis of Orm1 Phosphorylation

Strains harboring an Orm1-HA plasmid (pSH14HA) were grown to mid-log phase in synthetic medium minus histidine, and myriocin (0.15 μg/ml) was added for 1 hr. Orm1 phosphorylation was analyzed as previously described (Liu et al., 2012).

Spot Assays and Plasmid Shuffle

Spot assays were performed as previously described (Kats et al., 2009). Plasmid shuffle was performed as follows. *elo2*^{3A} *elo3Δ orm2Δ* triple-mutant cells harboring pBG1805-*ORM2* (a *URA3*-based plasmid containing *ORM2* under control of the *GAL1* promoter; Gelperin et al., 2005) were grown to log phase in dropout media lacking uracil and with 2% raffinose and 0.5% galactose as the carbon source (to express *ORM2*). Cells were then spotted on synthetic complete media containing 2% raffinose/0.5% galactose in the absence or presence of 1 mg/ml 5-fluoroorotic acid (5-FOA) as indicated in the figure.

Lipid Extraction and Analysis Of Lipid Content

Yeast strains were grown in rich medium until log phase and 25 OD pellets were harvested. Briefly, glycerophospholipids and sphingolipids were extracted with pyridine-ethanol-diethylether-water solvent. Sphingolipids were base-treated with monomethylamine solvent. Both lipid classes were desalted with n-butanol and analyzed by electrospray ionization MS as previously described (Guan et al., 2010). Synthetic internal standards were spiked to the cell pellets prior to extraction: Cer d18:0/17:0 (0.24 nmol), GlcCer d18:1/8:0 (4 nmol), C17 sphingosine (3.75 μg), and C17 sphingosine 1-phosphate (3.75 μg) (Avanti Polar Lipids). The assays were performed with three independent biological replicates. LCBs and LCBPs were analyzed as described in Supplemental Information.

Microscopy

Live cell microscopy was performed as previously described (Enserink et al., 2006). Cells expressing GFP-Atg8, red fluorescent protein-Atg8, or GFP-Ape1 were imaged using a Zeiss Axioplan 2 microscope equipped with a 63×/1.40 Oil Plan-Apochromat objective (Zeiss), using a charge-coupled device camera (Zeiss AxioCam Hrc) and AxioVision Rel. 4.6 software (Zeiss),

and images were processed using Photoshop and Illustrator software (both Adobe).

Autophagy Assays

Autophagy was studied using previously described methods (Cheong and Klionsky, 2008; Shintani and Reggiori, 2008). See Supplemental Information for details.

Viable Cell Count

Cell viability assays were performed as previously described (Enserink et al., 2006).

Statistical Methods

All experiments were performed at least three times, and p values were calculated with the Student's t test.

SUPPLEMENTAL INFORMATION

Supplemental information includes Supplemental Experimental Procedures, four figures, and three tables and can be found with this article online at http://dx.doi.org/10.1016/j.celrep.2013.10.024.

ACKNOWLEDGMENTS

We gratefully acknowledge Drs. K. Cunningham, D. Klionsky, Y. Ohsumi, and H. Takematsu for reagents, E. Lång for assistance with fluorescence microscopy, and T. de Kroon and R. Loewith for helpful comments. J.M.E. is supported by Helse Sør-Øst grant 2010036, Norwegian Research Council grant 221694/F20, and by Norwegian Cancer Society grant 331178260260. P.C. is supported by Norwegian Research Council grant 221920/F20. H.R. is supported by the NCCR Chemical Biology, SystemsX.ch (LipidX.ch), evaluated by the Swiss National Science Foundation (SNSF) and a grant (146142) from the SNSF. N.J.F. is supported by The Danish Council for Independent Research, Natural Sciences grant no. 23459.

Received: May 16, 2013
Revised: September 12, 2013
Accepted: October 11, 2013
Published: November 14, 2013

REFERENCES

Aguilar, P.S., Fröhlich, F., Rehman, M., Shales, M., Ulitsky, I., Olivera-Couto, A., Braberg, H., Shamir, R., Walter, P., Mann, M., et al. (2010). A plasma-membrane E-MAP reveals links of the eisosome with sphingolipid metabolism and endosomal trafficking. Nat. Struct. Mol. Biol. *17*, 901–908.

Aronova, S., Wedaman, K., Aronov, P.A., Fontes, K., Ramos, K., Hammock, B.D., and Powers, T. (2008). Regulation of ceramide biosynthesis by TOR complex 2. Cell Metab. *7*, 148–158.

Baba, M., Osumi, M., Scott, S.V., Klionsky, D.J., and Ohsumi, Y. (1997). Two distinct pathways for targeting proteins from the cytoplasm to the vacuole/lysosome. J. Cell Biol. *139*, 1687–1695.

Barbet, N.C., Schneider, U., Helliwell, S.B., Stansfield, I., Tuite, M.F., and Hall, M.N. (1996). TOR controls translation initiation and early G1 progression in yeast. Mol. Biol. Cell *7*, 25–42.

Berchtold, D., Piccolis, M., Chiaruttini, N., Riezman, I., Riezman, H., Roux, A., Walther, T.C., and Loewith, R. (2012). Plasma membrane stress induces relocalization of Slm proteins and activation of TORC2 to promote sphingolipid synthesis. Nat. Cell Biol. *14*, 542–547.

Breslow, D.K., Collins, S.R., Bodenmiller, B., Aebersold, R., Simons, K., Shevchenko, A., Ejsing, C.S., and Weissman, J.S. (2010). Orm family proteins mediate sphingolipid homeostasis. Nature *463*, 1048–1053.

Broach, J.R. (2012). Nutritional control of growth and development in yeast. Genetics *192*, 73–105.

Cheong, H., and Klionsky, D.J. (2008). Biochemical methods to monitor autophagy-related processes in yeast. Methods Enzymol. *451*, 1–26.

Cybulski, N., and Hall, M.N. (2009). TOR complex 2: a signaling pathway of its own. Trends Biochem. Sci. *34*, 620–627.

Daub, H., Olsen, J.V., Bairlein, M., Gnad, F., Oppermann, F.S., Körner, R., Greff, Z., Kéri, G., Stemmann, O., and Mann, M. (2008). Kinase-selective enrichment enables quantitative phosphoproteomics of the kinome across the cell cycle. Mol. Cell *31*, 438–448.

De Virgilio, C., and Loewith, R. (2006). Cell growth control: little eukaryotes make big contributions. Oncogene *25*, 6392–6415.

Denic, V., and Weissman, J.S. (2007). A molecular caliper mechanism for determining very long-chain fatty acid length. Cell *130*, 663–677.

Dickson, R.C. (2008). Thematic review series: sphingolipids. New insights into sphingolipid metabolism and function in budding yeast. J. Lipid Res. *49*, 909–921.

Ejsing, C.S., Sampaio, J.L., Surendranath, V., Duchoslav, E., Ekroos, K., Klemm, R.W., Simons, K., and Shevchenko, A. (2009). Global analysis of the yeast lipidome by quantitative shotgun mass spectrometry. Proc. Natl. Acad. Sci. USA *106*, 2136–2141.

Enserink, J.M., Smolka, M.B., Zhou, H., and Kolodner, R.D. (2006). Checkpoint proteins control morphogenetic events during DNA replication stress in Saccharomyces cerevisiae. J. Cell Biol. *175*, 729–741.

Enserink, J.M., Hombauer, H., Huang, M.E., and Kolodner, R.D. (2009). Cdc28/Cdk1 positively and negatively affects genome stability in S. cerevisiae. J. Cell Biol. *185*, 423–437.

Flores-Rozas, H., and Kolodner, R.D. (1998). The Saccharomyces cerevisiae MLH3 gene functions in MSH3-dependent suppression of frameshift mutations. Proc. Natl. Acad. Sci. USA *95*, 12404–12409.

Gable, K., Han, G., Monaghan, E., Bacikova, D., Natarajan, M., Williams, R., and Dunn, T.M. (2002). Mutations in the yeast LCB1 and LCB2 genes, including those corresponding to the hereditary sensory neuropathy type I mutations, dominantly inactivate serine palmitoyltransferase. J. Biol. Chem. *277*, 10194–10200.

Gallego, O., Betts, M.J., Gvozdenovic-Jeremic, J., Maeda, K., Matetzki, C., Aguilar-Gurrieri, C., Beltran-Alvarez, P., Bonn, S., Fernández-Tornero, C., Jensen, L.J., et al. (2010). A systematic screen for protein-lipid interactions in Saccharomyces cerevisiae. Mol. Syst. Biol. *6*, 430.

Gelperin, D.M., White, M.A., Wilkinson, M.L., Kon, Y., Kung, L.A., Wise, K.J., Lopez-Hoyo, N., Jiang, L., Piccirillo, S., Yu, H., et al. (2005). Biochemical and genetic analysis of the yeast proteome with a movable ORF collection. Genes Dev. *19*, 2816–2826.

Guan, X.L., Riezman, I., Wenk, M.R., and Riezman, H. (2010). Yeast lipid analysis and quantification by mass spectrometry. Methods Enzymol. *470*, 369–391.

Han, S., Lone, M.A., Schneiter, R., and Chang, A. (2010). Orm1 and Orm2 are conserved endoplasmic reticulum membrane proteins regulating lipid homeostasis and protein quality control. Proc. Natl. Acad. Sci. USA *107*, 5851–5856.

He, C., and Klionsky, D.J. (2009). Regulation mechanisms and signaling pathways of autophagy. Annu. Rev. Genet. *43*, 67–93.

Kamada, Y., Funakoshi, T., Shintani, T., Nagano, K., Ohsumi, M., and Ohsumi, Y. (2000). Tor-mediated induction of autophagy via an Apg1 protein kinase complex. J. Cell Biol. *150*, 1507–1513.

Kats, E.S., Enserink, J.M., Martinez, S., and Kolodner, R.D. (2009). The Saccharomyces cerevisiae Rad6 postreplication repair and Siz1/Srs2 homologous recombination-inhibiting pathways process DNA damage that arises in asf1 mutants. Mol. Cell. Biol. *29*, 5226–5237.

Kim, S., Fyrst, H., and Saba, J. (2000). Accumulation of phosphorylated sphingoid long chain bases results in cell growth inhibition in Saccharomyces cerevisiae. Genetics *156*, 1519–1529.

Kinoshita, E., Kinoshita-Kikuta, E., Takiyama, K., and Koike, T. (2006). Phosphate-binding tag, a new tool to visualize phosphorylated proteins. Mol. Cell. Proteomics *5*, 749–757.

Kobayashi, S.D., and Nagiec, M.M. (2003). Ceramide/long-chain base phosphate rheostat in Saccharomyces cerevisiae: regulation of ceramide synthesis by Elo3p and Cka2p. Eukaryot. Cell *2*, 284–294.

Kunz, J., Henriquez, R., Schneider, U., Deuter-Reinhard, M., Movva, N.R., and Hall, M.N. (1993). Target of rapamycin in yeast, TOR2, is an essential phosphatidylinositol kinase homolog required for G1 progression. Cell *73*, 585–596.

Lavieu, G., Scarlatti, F., Sala, G., Carpentier, S., Levade, T., Ghidoni, R., Botti, J., and Codogno, P. (2006). Regulation of autophagy by sphingosine kinase 1 and its role in cell survival during nutrient starvation. J. Biol. Chem. *281*, 8518–8527.

Lee, J., Moir, R.D., McIntosh, K.B., and Willis, I.M. (2012). TOR signaling regulates ribosome and tRNA synthesis via LAMMER/Clk and GSK-3 family kinases. Mol. Cell *45*, 836–843.

Liu, C., Apodaca, J., Davis, L.E., and Rao, H. (2007). Proteasome inhibition in wild-type yeast Saccharomyces cerevisiae cells. Biotechniques *42*, 158, 160, 162.

Liu, M., Huang, C., Polu, S.R., Schneiter, R., and Chang, A. (2012). Regulation of sphingolipid synthesis through Orm1 and Orm2 in yeast. J. Cell Sci. *125*, 2428–2435.

Loewith, R., Jacinto, E., Wullschleger, S., Lorberg, A., Crespo, J.L., Bonenfant, D., Oppliger, W., Jenoe, P., and Hall, M.N. (2002). Two TOR complexes, only one of which is rapamycin sensitive, have distinct roles in cell growth control. Mol. Cell *10*, 457–468.

Michelmore, R.W., Paran, I., and Kesseli, R.V. (1991). Identification of markers linked to disease-resistance genes by bulked segregant analysis: a rapid method to detect markers in specific genomic regions by using segregating populations. Proc. Natl. Acad. Sci. USA *88*, 9828–9832.

Nagiec, M.M., Skrzypek, M., Nagiec, E.E., Lester, R.L., and Dickson, R.C. (1998). The LCB4 (YOR171c) and LCB5 (YLR260w) genes of Saccharomyces encode sphingoid long chain base kinases. J. Biol. Chem. *273*, 19437–19442.

Niles, B.J., Mogri, H., Hill, A., Vlahakis, A., and Powers, T. (2012). Plasma membrane recruitment and activation of the AGC kinase Ypk1 is mediated by target of rapamycin complex 2 (TORC2) and its effector proteins Slm1 and Slm2. Proc. Natl. Acad. Sci. USA *109*, 1536–1541.

Noda, T., and Ohsumi, Y. (1998). Tor, a phosphatidylinositol kinase homologue, controls autophagy in yeast. J. Biol. Chem. *273*, 3963–3966.

Nugteren, D.H. (1965). The enzymic chain elongation of fatty acids by rat-liver microsomes. Biochim. Biophys. Acta *106*, 280–290.

Oh, C.S., Toke, D.A., Mandala, S., and Martin, C.E. (1997). ELO2 and ELO3, homologues of the Saccharomyces cerevisiae ELO1 gene, function in fatty acid elongation and are required for sphingolipid formation. J. Biol. Chem. *272*, 17376–17384.

Orsi, A., Polson, H.E., and Tooze, S.A. (2010). Membrane trafficking events that partake in autophagy. Curr. Opin. Cell Biol. *22*, 150–156.

Pultz, D., Bennetzen, M.V., Rødkær, S.V., Zimmermann, C., Enserink, J.M., Andersen, J.S., and Færgeman, N.J. (2012). Global mapping of protein phosphorylation events identifies Ste20, Sch9 and the cell-cycle regulatory kinases Cdc28/Pho85 as mediators of fatty acid starvation responses in Saccharomyces cerevisiae. Mol. Biosyst. *8*, 796–803.

Revardel, E., Bonneau, M., Durrens, P., and Aigle, M. (1995). Characterization of a new gene family developing pleiotropic phenotypes upon mutation in Saccharomyces cerevisiae. Biochim. Biophys. Acta *1263*, 261–265.

Roelants, F.M., Breslow, D.K., Muir, A., Weissman, J.S., and Thorner, J. (2011). Protein kinase Ypk1 phosphorylates regulatory proteins Orm1 and Orm2 to control sphingolipid homeostasis in Saccharomyces cerevisiae. Proc. Natl. Acad. Sci. USA *108*, 19222–19227.

Saba, J.D., Nara, F., Bielawska, A., Garrett, S., and Hannun, Y.A. (1997). The BST1 gene of Saccharomyces cerevisiae is the sphingosine-1-phosphate lyase. J. Biol. Chem. *272*, 26087–26090.

Shimobayashi, M., Oppliger, W., Moes, S., Jenö, P., and Hall, M.N. (2013). TORC1-regulated protein kinase Npr1 phosphorylates Orm to stimulate complex sphingolipid synthesis. Mol. Biol. Cell *24*, 870–881.

Shintani, T., and Reggiori, F. (2008). Fluorescence microscopy-based assays for monitoring yeast Atg protein trafficking. Methods Enzymol. *451*, 43–56.

Song, C., Ye, M., Liu, Z., Cheng, H., Jiang, X., Han, G., Songyang, Z., Tan, Y., Wang, H., Ren, J., et al. (2012). Systematic analysis of protein phosphorylation networks from phosphoproteomic data. Mol. Cell. Proteomics *11*, 1070–1083.

Tabuchi, M., Audhya, A., Parsons, A.B., Boone, C., and Emr, S.D. (2006). The phosphatidylinositol 4,5-biphosphate and TORC2 binding proteins Slm1 and Slm2 function in sphingolipid regulation. Mol. Cell. Biol. *26*, 5861–5875.

Villén, J., Beausoleil, S.A., Gerber, S.A., and Gygi, S.P. (2007). Large-scale phosphorylation analysis of mouse liver. Proc. Natl. Acad. Sci. USA *104*, 1488–1493.

Wilson-Grady, J.T., Villén, J., and Gygi, S.P. (2008). Phosphoproteome analysis of fission yeast. J. Proteome Res. *7*, 1088–1097.

Yorimitsu, T., Zaman, S., Broach, J.R., and Klionsky, D.J. (2007). Protein kinase A and Sch9 cooperatively regulate induction of autophagy in Saccharomyces cerevisiae. Mol. Biol. Cell *18*, 4180–4189.

Young, M.M., Kester, M., and Wang, H.G. (2013). Sphingolipids: regulators of crosstalk between apoptosis and autophagy. J. Lipid Res. *54*, 5–19.

Zhang, H.H., Lipovsky, A.I., Dibble, C.C., Sahin, M., and Manning, B.D. (2006). S6K1 regulates GSK3 under conditions of mTOR-dependent feedback inhibition of Akt. Mol. Cell *24*, 185–197.

Zimmermann, C., Chymkowitch, P., Eldholm, V., Putnam, C.D., Lindvall, J.M., Omerzu, M., Bjørås, M., Kolodner, R.D., and Enserink, J.M. (2011). A chemical-genetic screen to unravel the genetic network of CDC28/CDK1 links ubiquitin and Rad6-Bre1 to cell cycle progression. Proc. Natl. Acad. Sci. USA *108*, 18748–18753.